Research Article Vol. 62, No. 1 / 1 January 2023 / Applied Optics 217

applied optics

Design and optimization of the tripod flexure for a 2m lightweight mirror for space application

Ping Jiang, Chuang Xue,* Kejun Wang, Xiaoyu Wang, and Pingwei Zhou

Changchun Institute of Optics, Fine Mechanics and Physics, Chinese Academy of Sciences, Dong-Nanhu Road 3888, Changchun 130033, China
**Corresponding author: popxue2022@163.com*

Received 27 September 2022; revised 27 November 2022; accepted 2 December 2022; posted 5 December 2022; published 19 December 2022

In order to ensure optimal optical performance, primary mirror assembly must be impervious to environmental influences. These environmental influences include gravity, assembly error, and thermal change, under which external loads are imposed on the mirror. The external loads degrade the mirror surface accuracy and cause misalignment between mirrors. In this paper, a tripod flexure with a flexible hinge is designed to alleviate the influence of the external load on the surface accuracy of a 2 m primary mirror. This structure can effectively release the rotational freedom, provide a certain translational flexibility, and yield high axial stiffness. The axial stiffness is used to increase the frequency of the primary mirror assembly. According to the fast optimization model, the derivation of close form compliance equations is developed to characterize the flexibility, and parameter optimization is done to achieve the maximum performance. Then a finite element analysis and test are used to verify the final design. The results show that the index requirements of the 2 m primary mirror have been met.

https://doi.org/10.1364/AO.476783

1. INTRODUCTION

In a space-based telescope, there is a trend of using large-aperture reflective mirrors to improve the angular resolution and signal-to-noise ratios [1–5]. As the size of the mirror increases, the support structure design undoubtedly becomes one of the challenges in the design of space telescopes. The structural form of the flexible hinge provides more possibilities for mirror support design. As a special transmission structure, the flexure hinge provides a small range of translation or rotation between adjacent components through elastic deformation. Different flexibility configurations determine the performance of flexure hinges under static loads [6]. The flexure hinge design method based on a flexibility equation was first proposed by Paro and Weisbord, and then a variety of flexure hinges were designed. Since then, the flexure hinge has received more interest from scholars. Many new configurations of flexure hinges have been proposed using analytical methods. Smith *et al*. proposed an elliptical flexure hinge by extrapolating the cut curve from a circle to an ellipse [7]. Lobontiu *et al*. derived the exact flexibility equation of an angular circular flexure hinge [8–10]. Moreover, a set of flexure hinge design methods based on the flexibility equation was introduced by quantifying rotation capacity, rotation accuracy, and stress level [11]. The configuration of the flexure hinge has been developed from two-dimensional to three-dimensional, and from a simple to complex structure, such as cartwheel hinge [12]. At present, flexure hinges are widely used in aerospace, manufacturing, optics, and other fields.

Flexible hinges are becoming more widely used in the field of space telescope design, especially in the mirror support design. When designing a flexible support for a mirror, a suitable flexible hinge is determined to take into account many practical factors, including the mirror weight, lightweight form, external loads, assembly errors, processing technology, and the position of the hinge in the flexible support. The flexible support may contain one or more types of flexible hinges. The type of hinges can be determined according to different functional requirements.

For the design of a mirror support structure, the two most extensively used mounts are the flexure bipod mounts [13–16] and flexure hinge mounts [17–21]. Due to the peculiarities of the flexure bipod, the subtle deviation will cause substantial degradation of the mirror performance. Moreover, even if it is possible to compensate for the gravitational distortion of the mirror, the implemented method is quite complicated. The flexure bipod must be long enough to release the deformation of the mirror caused by temperature variation and assembly tolerance; the mirror will be far away from the space telescope base plate. Thus, a flexure bipod will increase the axial envelope size of the mirror assembly. A method that assembles the flexure hinge mounts on the back blind hole of the mirror was adopted. This method has been implemented on many different apertures of mirrors in their studies, where the invar sleeve is attached to the mount with a flexure to match the coefficient

of thermal expansion of the mirror material. The back support structure has the advantages of light weight and small space occupation. When the comprehensive surface of mirror assembly is decomposed into gravity, temperature, and axial assembly stress according to the actual working conditions, the surface accuracy under the action of temperature and axial assembly stress is required to be high. In general, it is difficult to balance the contradiction between the surface shape, fundamental frequency, and dynamic stress of the traditional flexible support under the above working conditions. In addition, the traditional flexible support design is more inclined to trial and error, the design direction is not clear enough, and the efficiency is low.

A fast design method of the flexible support is proposed by Zhou and Xu [22]. In this paper, they describe a method to determine the allowable external loads. The performance of a flexure is evaluated by the transmitted loads to the mirror. The force acting on the mirror was analyzed under various conditions, and the influence functions were obtained using inertia relief. With the knowledge of influence functions, the relationship between external loads and mirror surface distortion was built. According to the error budget of the primary mirror, the permissible loads required of the flexure were directly established. The optimization was achieved through optimizing the compliance of the flexure without a mirror. With their method, the mirror design and flexure design were decoupled, and time and resources required for optimization were reduced. A parallel flexure is demonstrated for a 2 m lightweight, horizontally supported mirror in their research. The influence of gravity, assembly error, and temperature conditions on the mirror surface shape and frequency is analyzed quantitatively, and the flexibility requirements of the flexible support under different conditions are obtained.

When designing the flexible support for large-diameter mirrors based on the principle of three-point support on the back in order to reduce the surface shape error under gravity and assembly errors, the flexible support needs to release the rotational freedom. Under the influence of temperature change, the flexible support should release its translation freedom. However, to limit the decenter of the primary mirror under gravity, this translation flexibility should not be large. Generally, the primary mirror can be easily affected by bending, but not by shear [17]. Then the surface error caused by shear force can often be ignored. The fundamental frequency of mirror assembly is related to the axial stiffness of flexure support. The axial stiffness of the flexible support should be kept or increased. Based on the above analysis, the flexure support should be a spherical flexure with high axial stiffness. Compared with the spherical joint, the spherical flexure has the advantages of no mechanical friction, no clearance, no hysteresis, and easy manufacture, assembly, adjustment, and maintenance.

In this paper, according to the flexibility requirements of 2 m mirror for flexible support under different working conditions given in Ref. [22], an inverted tripod flexure is designed to alleviate the influence of the external load on the surface accuracy of a 2 m primary mirror for space application. Based on the flexibility calculation formula, the topology of a flexure is proposed, and the closed-form compliance of the flexure is derived. The parameter optimization method is used to optimize the flexible support, and the structural parameters are determined. The finite element analysis is performed to verify the comprehensive performance of the primary mirror assembly. Finally, the compliance of the designed flexure is tested.

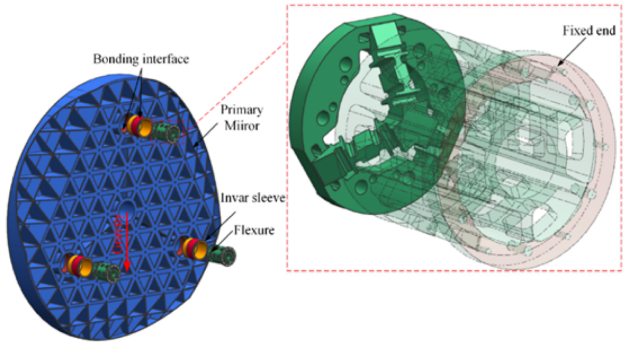

Fig. 1. Exploded view of a pre-designed lightweight primary mirror assembly showing the symmetries, invar sleeve, and gravity orientation. For clarity, the rigid part of the flexure has been set to transparent.

2. MIRROR AND SUPPORT CONFIGURATION

In this study, a 2 m partially closed back monolithic, silicon carbide (SiC) primary mirror configuration is examined [22]. The radius of curvature is 10.5 m, the supporting radius is 0.68 m, the depth is 0.18 m, and the mass is 265 kg. To improve the thermal stability, three invar sleeves, which have the same expansion coefficient with SiC material, are bonded to the internal surface of supporting holes using epoxy adhesive (GHJ-01(Z)) in a 120-degree interval. The primary mirror is supported by three parallel flexures through the supporting holes located on its back, as shown in Fig. 1; the material properties used in the primary mirror assembly are summarized in Table 1. The flexible support may be regarded as a semi-kinematic design because it has a finite contact area. Three-point support is commonly used in the mirror support of space telescopes due to its simplicity and effectiveness. As the primary mirror subassembly and the telescope are tested and aligned with a horizontal optical axis, the required self-weight distortions can be achieved by three-point supports. Meanwhile, minimizing self-weight distortions on flight mounts without gravity unloading using counterweights, airbags, or actuators introduces the least uncertainty to test.

According to the type of external disturbance [23], a comprehensive surface figure (RMS) of 7.8 nm is decomposed into 5 nm for gravity effect, in which the distortion of a single mirror is less than 4.5 nm, and the distortion of the support is not more than 2.6 nm; The surface distortion caused by the assembly error is less than 4 nm, which mainly refers to the surface accuracy degradation when the flatness error of the mounting surface of the primary mirror assembly is 0.1 mm. When the temperature changes 4°C, 4.8 nm degradation of RMS is allowed, as shown in Fig. 2.

Table 1. Performance and Constraints of the Mirror Assembly under Different Operating Conditions

Material	SiC (Mirror)	Invar (Sleeve)	Titanium (Flexure)	Adhesive
Yong's modulus (Mpa)	330	141	109	0.158
Poisson's ration	0.25	0.25	0.29	0.49
Density (t/mm^3)	3.05×10^{-9}	8.1×10^{-9}	4.4×10^{-9}	1.3×10^{-9}
Coefficient of thermal expansion (/°C)	2.5×10^{-6}	2.5×10^{-6}	9.1×10^{-6}	3×10^{-3}

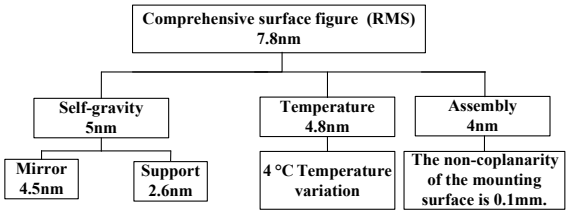

Fig. 2. Schematic illustration of the performance metrics.

3. DESIGN OF FLEXIBLE SUPPORT BASED ON FLEXIBILITY EQUATION

A. Topology Design of Flexible Support

Due to the requirement on the optical performance, the primary mirror assembly must have the ability to be unaffected by environmental influences. These environmental influences include gravity, assembly error, and thermal change, under which external loads are imposed on the mirror. The external loads degrade the mirror surface accuracy and cause misalignment between mirrors. The flexure is used to isolate external loads by passively utilizing its own elastic deformation. Thus, the optical supporting performance of a flexure can be evaluated by the transmitted loads to the mirror. The relationship between the displacements at the free end and the transmitted loads can be formulated as follows:

$$\left[u_x\ u_y\ u_z\ \theta_x\ \theta_y\ \theta_z\right]^T = C\left[F_x\ F_y\ F_z\ M_x\ M_y\ M_z\right]^T, \quad (1)$$

where F_n and u_n represent the force and linear displacement along the three coordinate axes, respectively; M_n and θ_n represent the bending moment and angular displacement around the three coordinate axes, respectively, and C is the flexibility matrix.

A few remarks will be made in the following regarding the application of Eq. (1) to the analysis of the flexure. First, the flexure mounting is composed of flexible strips and a rigid part in which the flexible strips are much more flexible than its connecting parts; that is, the deflection due to shearing is negligible. Secondly, the flexure strips are assumed to be homogeneous and isotropic. Finally, the compliance matrix C is developed by utilizing Castigliano's displacement theorem, which is formulated based on the strain energy stored through elastic deformations. The compliance matrix C, which includes 10 independent elements [24–26], is shown as follows:

$$C = \begin{bmatrix} C_{x-F_x} & 0 & 0 & 0 & 0 & 0 \\ 0 & C_{y-F_y} & 0 & 0 & 0 & C_{y-M_z} \\ 0 & 0 & C_{z-F_z} & 0 & C_{z-M_y} & 0 \\ 0 & 0 & 0 & C_{\theta_x-M_x} & 0 & 0 \\ 0 & 0 & C_{\theta_y-F_z} & 0 & C_{\theta_y-M_y} & 0 \\ 0 & C_{\theta_z-F_y} & 0 & 0 & 0 & C_{\theta_z-M_z} \end{bmatrix}. \quad (2)$$

Flexible spherical joints can effectively ensure the mirror surface accuracy and structural stability, and have high adaptability to external environmental disturbances. The topology of the flexible spherical joint adopts a multi-axis hinge combined with a parallel tripod, as shown in Fig. 3(a). In order to improve the stability of the flexible spherical joint, the traditional thin rod structure is replaced by the spring structure with equivalent flexibility, as shown in Fig. 3(b). In order to reduce the local thermal stress caused by the mismatch of the linear expansion coefficient between the invar cone sleeve and titanium alloy flexible support, the flexible moving pair shown in Fig. 3(c) is adopted. The topology of flexible support is shown in Fig. 3(d). The flexible part is composed of three legs, and each leg is composed of two Hooke hinges (U) and a moving pair (P). In order to make the rotation center of the flexible support (the zero moment point of the flexible joint) coincide with the neutral plane of the mirror,

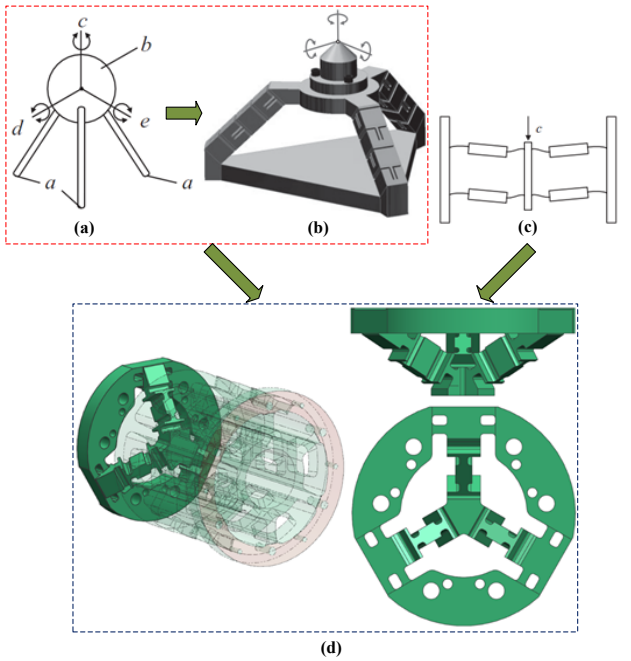

Fig. 3. Topology structure of the flexure support for the 2 m primary mirror. (a) Tripod spherical hinge with a wire flexure. (b) Tripod spherical hinge with a blade flexure. (c) Translation flexure hinge. (d) Topology structure of the flexure support for the 2 m primary mirror.

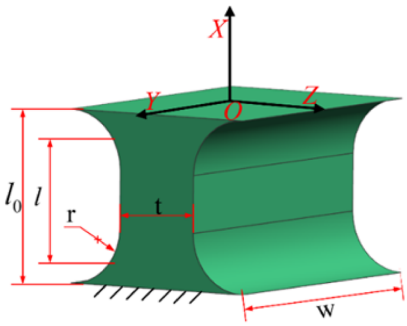

Fig. 4. Size of the basic compliant elements.

the inverted tripod structure is adopted. The rest of the structure of flexible support is defined as the rigid part, which plays the role of connection. The topology of the flexible support (3PUU) can provide rotational flexibility and translational flexibility, and it has high axial stiffness.

B. Flexibility Calculation Method

Due to the limited flexible support space and high axial stiffness demand of the large-aperture mirror, the length and thickness of the flexible element are similar, and the flexibility matrix obtained by a direct derivation has a large error with the finite element method. The flexibility matrix of the angular circular flexure hinge was too complex to optimize the flexible support. The fillet radius of the flexible support is far less than the length of the flexible element, so the flexibility equation of the straight beam hinge is adopted in this paper. The research shows that, when the error between the calculation equation and the finite element result is less than 10%, the calculation equation can be used to guide the engineering design [27].

The flexible element of the flexible support is usually a short beam, and the torsion and shear deformation should be considered in the calculation. The structural dimensions and coordinate system of the flexible unit are shown in Fig. 4. In order to improve the calculation accuracy, the length of the flexible element is corrected as

$$l = l_0 - r, \tag{3}$$

where l_0 is the length of the flexible unit, and r is the fillet radius.

The relationship between the flexibility matrix of the straight beam hinge and structural size is as follows:

$$C = \begin{bmatrix} \frac{l}{EA} & 0 & 0 & 0 & 0 & 0 \\ 0 & \frac{l^3}{3EI_z} + \frac{f_s l}{GA} & 0 & 0 & 0 & \frac{l^2}{2EI_z} \\ 0 & 0 & \frac{l^3}{3EI_y} + \frac{f_s l}{GA} & 0 & \frac{-l^2}{2EI_y} & 0 \\ 0 & 0 & 0 & \frac{l}{GJ} & 0 & 0 \\ 0 & 0 & \frac{-l^2}{2EI_y} & 0 & \frac{l}{EI_y} & 0 \\ 0 & \frac{l^2}{2EI_z} & 0 & 0 & 0 & \frac{l}{EI_z} \end{bmatrix}, \tag{4}$$

where E is the Young's modulus of the material, A is the cross-sectional area of the flexible unit, G is the shear modulus, f_s is the shear shape coefficient, and I_y, I_z, and J are the moments of inertia and torsion constants. The specific values of each parameter are

$$\begin{aligned} A &= wt \\ G &= E/(2(1+\nu)) \\ I_y &= wt^3/12 \\ I_z &= w^3 t/12 \\ J &= wt^3(1/3 - 0.21t/w(1 - 1/12(t/w)^4)), \end{aligned} \tag{5}$$

where w and t are the width and thickness of the flexure hinge, respectively.

The coordinate transformation method [28] is a general and fully parameterized analysis method for flexible structures. As shown in Fig. 5, if the flexibility matrix of the flexible element in the local coordinate system O_i is C_i (the stiffness matrix is K_i), the flexibility matrix can be transformed into the coordinate system O_j through a 6×6 coordinate transformation matrix T. The relationship between the flexibility matrix before and after conversion is

$$\begin{aligned} C_j &= TC_i T^T, \\ K_j &= T^{-T} K_i T^{-1} = T^{-T} C_i{}^{-1} T^{-1}, \end{aligned} \tag{6}$$

where the superscript t is expressed as a transpose matrix, and the coordinate transformation matrix can be expressed as

$$T = \begin{bmatrix} R & SR \\ 0 & R \end{bmatrix}, \tag{7}$$

where R represents the rotation matrix of coordinate system O_i relative to coordinate system O_j, and S represents the movement transformation matrix, and its expression is

$$R = \begin{bmatrix} \cos(\phi)\cos(\theta) & \cos(\phi)\sin(\theta)\sin(\psi) - \sin(\phi)\cos(\psi) & \cos(\phi)\sin(\theta)\sin(\psi) + \sin(\phi)\sin(\psi) \\ \sin(\phi)\cos(\theta) & \sin(\phi)\sin(\theta)\sin(\psi) + \cos(\phi)\cos(\psi) & \sin(\phi)\sin(\theta)\cos(\psi) - \cos(\phi)\sin(\psi) \\ -\sin(\theta) & \cos(\theta)\sin(\psi) & \cos(\theta)\cos(\psi) \end{bmatrix}$$

$$S = \begin{bmatrix} 0 & -r_z & r_y \\ r_z & 0 & -r_x \\ -r_y & r_x & 0 \end{bmatrix}. \tag{8}$$

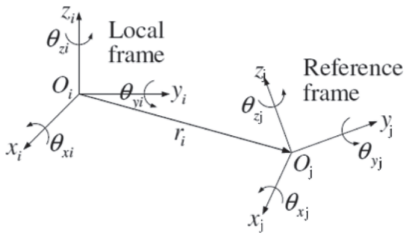

Fig. 5. Representation of compliance transformation.

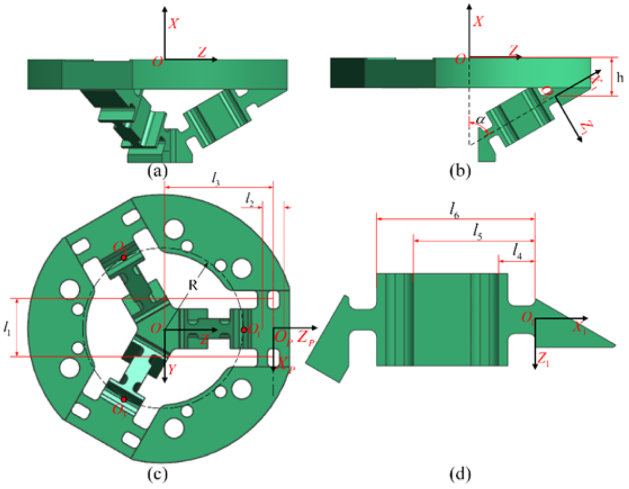

Fig. 6. Combination structure of a tripod flexure with three identical chains.

When the flexible elements are represented in the same coordinate system, the flexibility of the series flexible structure is equal to the sum of the flexibility of each element; that is, $C = \sum_{i=1} T_i C_i T_i^T$. The stiffness of the parallel flexible structure is equal to the sum of the stiffness of each element; that is, $K = \sum_{i=1} T_i^{-T} K_i T_i^{-1}$.

C. Flexibility Calculation of Moving Pair

As shown in Fig. 6, O_P is defined as the origin of the moving pair coordinate system, which is located in the same plane as the origin O of the global coordinate system, and the distance between them is l_3. Four parallel straight beam hinges form the moving pair 1. According to Eq. (8), the matrix parameters for converting the straight beam element coordinate system to the moving sub-coordinate system are

$$\begin{cases} T_1 = T(-(l_1 - l_p)/2,\ w_p/2,\ l_2/2,\ 0,\ 0,\ 0) \\ T_2 = T(-(l_1 - l_p)/2,\ w_p/2,\ -l_2/2,\ 0,\ 0,\ 0) \\ T_3 = T((l_1 - l_p)/2,\ w_p/2,\ l_2/2,\ 0,\ 0,\ -\pi) \\ T_4 = T((l_1 - l_p)/2,\ w_p/2,\ -l_2/2,\ 0,\ 0,\ -\pi) \end{cases}, \tag{9}$$

where l_p and w_p are the length and width of the straight beam hinge, respectively.

According to Eq. (6), the flexibility of the moving pair in hinge 1 is calculated as

$$C_{1P} = \left[\sum_{i=1}^{4} T_i^{-T} C_i^{-1} T_i^{-1} \right]^{-1}. \tag{10}$$

Similarly, the flexibility of the moving pair in hinges 2 and 3 is calculated, and the matrices of the three moving pair coordinate systems converted to the global coordinate coefficients, respectively, are

$$\begin{cases} T_1 = T(0,\ 0,\ l_3,\ 0,\ 0,\ \pi/2) \\ T_2 = T(0,\ -\sqrt{3}l_3/2,\ -l_3/2,\ 2\pi/3,\ 0,\ \pi/2) \\ T_3 = T(0,\ \sqrt{3}l_3/2,\ -l_3/2,\ -2\pi/3,\ 0,\ \pi/2) \end{cases}. \tag{11}$$

The flexibility of the moving pair in the global coordinate system is

$$C_{iP}^0 = T C_{iP} T^T, \tag{12}$$

where the superscript 0 represents the flexibility in the global coordinate system.

D. Hooke Hinge Flexibility Calculation

O_1 is defined as the origin of the rotating hinge in hinge 1, as shown in Fig. 6. The angle between the hinge and the flexible support axis is α, and the coordinates of X and Y in the global coordinate system are H and R, respectively. Two flexible Hooke hinges in hinge 1 are connected in a series, and each Hooke hinge includes two straight beam units connected in a series. According to Eq. (8), the transformation matrix parameters from the straight beam element coordinate system to the O_1 coordinate system are

$$\begin{cases} T_1 = T(0,\ 0,\ 0,\ 0,\ 0,\ 0) \\ T_2 = T(-l_4,\ 0,\ 0,\ \pi/2,\ 0,\ 0) \\ T_3 = T(-l_5,\ 0,\ 0,\ \pi/2,\ 0,\ 0) \\ T_4 = T(-l_6,\ 0,\ 0,\ \pi/2,\ 0,\ 0) \end{cases}. \tag{13}$$

According to Eq. (6), the flexibility of the two Hooke hinges in hinge 1 can be calculated as

$$C_{1U} = \sum_{i=1}^{4} T_i C_i T_i^T. \tag{14}$$

Similarly, the flexibility of the hook hinges in hinge 2 and branch chain 3 can be obtained. The transformation matrices from the Hooke hinge coordinate system to global coordinate system are

$$\begin{cases} T_1 = T(-h,\ 0,\ R,\ 0,\ -\alpha,\ 0) \\ T_2 = T(-h,\ -\sqrt{3}R/2,\ -R/2,\ 2\pi/3,\ -\alpha,\ 0) \\ T_3 = T(-h,\ \sqrt{3}R/2,\ -R/2,\ -2\pi/3,\ -\alpha,\ 0) \end{cases}. \tag{15}$$

The flexibility of the two Hooke hinges in the branch chain in the global coordinate system can be calculated as

$$C_{iU}^0 = T C_{iU} T^T, \tag{16}$$

where the superscript 0 represents the flexibility in the global coordinate system.

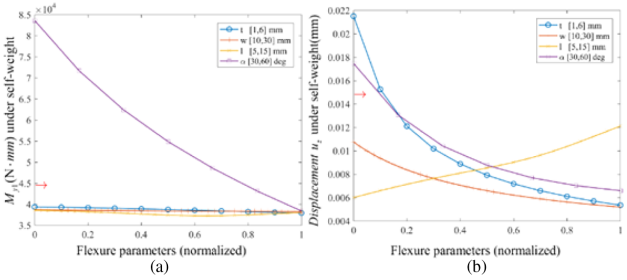

Fig. 7. Moment M_{y1} and displacement u_z of the primary mirror assembly under 1 g gravity with respect to the flexure parameters.

E. Flexibility Calculation and Analysis of Flexible Support

Each hinge is composed of a moving pair and two Hooke hinges in a series. The flexibility of a single hinge in the global coordinate system can be calculated as

$$C_i^0 = C_{iP} + C_{iU}. \tag{17}$$

The three hinges of the flexible support are connected in parallel, and the flexibility can be calculated as

$$C^0 = \left[\sum_{i=1}^{3} [C_i^0]^{-1}\right]^{-1}. \tag{18}$$

$R = 46$ mm, according to the diameter of the mirror support hole. The thickness of the flange plate at the front end of the flexible support is 15 mm, and h is 16 mm according to engineering experience. Figure 6 shows the curve of the bending moment M_{y1} [22] and rigid body displacement u_z of the mirror under the gravity condition with each parameter. When other parameters are fixed at the nominal value [29]. The nominal values of flexure hinge thickness t, width w, length l, and included angle α are 4, 20, and 6 mm, and 60°, respectively. Each parameter is normalized in Fig. 7, and the range of actual values is shown in the legend. The requirements of M_{y1} under the gravity condition are indicated by red arrows. Except for the included angle α value being low, other parameter ranges meet the requirements, as shown in Fig. 7(a). The greater the slope of the curve, the greater is the influence of the parameters on the target. Included angle α is the most sensitive parameter, and its tolerance needs to be strictly controlled. The requirements of u_z under the gravity condition are indicated by a red arrow. Except for thickness t and width w, other parameter ranges meet the requirements, as shown in Fig. 7(b). Rigid body displacement u_z is directly proportional to the length l and inversely proportional to other parameters.

Figure 8 shows the curve of the bending moment M_{y1} of the mirror under the condition of the 0.1 mm assembly error with each parameter, when other parameters are fixed at the nominal value. The variation range of most parameters meets the requirements of the bending moment, but the thickness t should be small enough to meet the requirements. Figure 9 shows the curve of β with each parameter under the temperature condition, when other parameters are fixed at the nominal value. Except for the included angle α value being low, the variation range of other parameters meets the requirements. Comparing

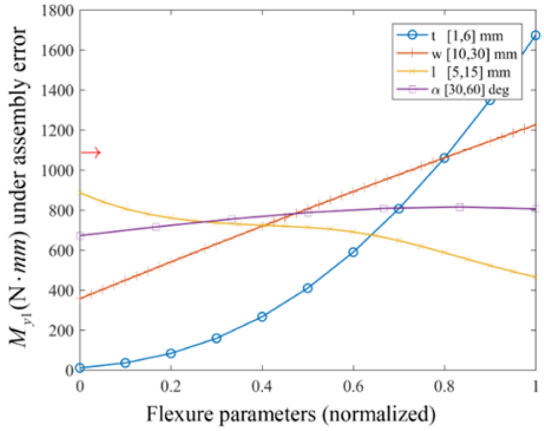

Fig. 8. Moment M_{y1} under a 0.1 mm assembly error with respect to the flexure parameters.

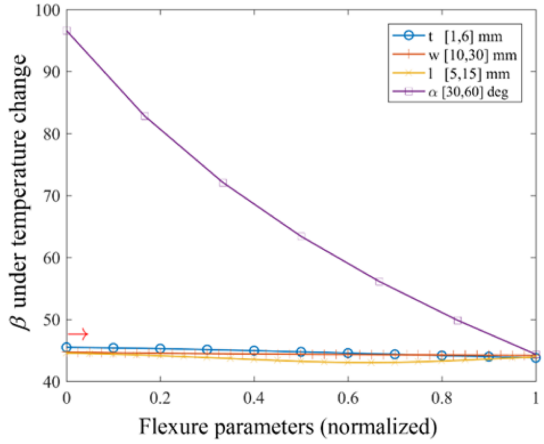

Fig. 9. Ratio β under 4°C temperature change with respect to flexure parameters.

Figs. 7(a) and 9, it can be seen that the design parameters have the same influence on the mirror bending moment M_{y1} under the gravity condition and β under the temperature condition. According to this characteristic, the two design objectives can be combined in design and optimization.

In the vibration test, the mirror assembly will be excited in three directions. The first-order frequency appears in the direction of maximum flexibility. By comparing the flexibility of the first three columns of Eq. (2), the fundamental frequency of the mirror assembly can be obtained. Figure 10 shows the curve of the first-order translational frequency of the mirror assembly with each parameter when other parameters are fixed at the nominal value. As can be seen from Fig. 10, most parameter ranges meet the requirements of frequency higher than 100 Hz, but the thickness t and angle should be large enough to meet the requirements.

4. PARAMETRIC DESIGN

There is an error between the closed flexibility equation and the finite element method. The design accuracy can be improved by using the finite element method. The flexible support parameter optimization link built by the integrated optimization software

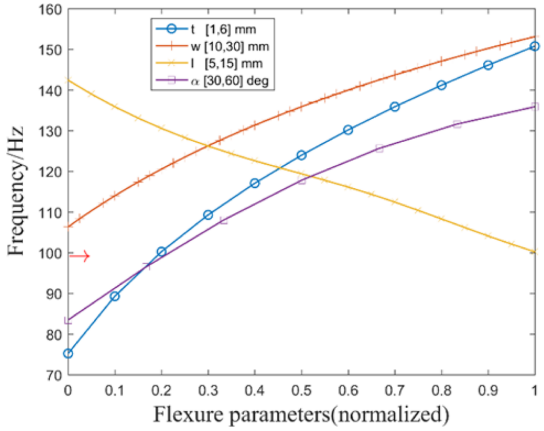

Fig. 10. First natural frequency with respect to flexure parameters.

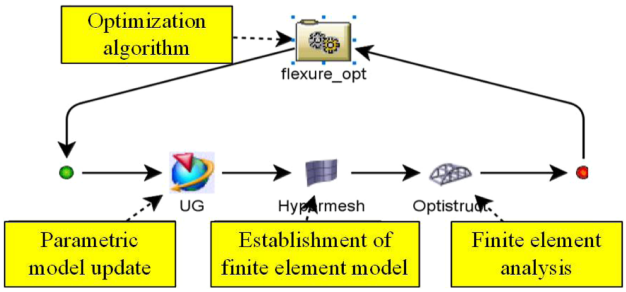

Fig. 11. iSIGHT linkage of flexure optimization.

iSIGHT is shown in Fig. 11. Integrate UG, HyperMesh, and Optistruct software through sight, and set the variables listed in Table 1 as the optimization variables. The specific optimization process includes:

(1) Using C language to develop and compile the ugupdate.exe program to update the UG parametric model and export the Parasolid format model;
(2) Writing TCL script to call HyperMesh software to realize geometric model import, geometric model cleaning, tet10 mesh drawing, material and element attribute distribution, boundary conditions and load application, and finally submit it to Opistruct software for a finite element analysis;
(3) According to the analysis results, iSIGHT calls the built-in optimization strategy to complete multiple iterations.

After 120 iterations, the sensitivity, design space, and optimal solution of each design variable to the target were obtained. Through a sensitivity analysis, the sensitivity of each design variable to the objective function is shown in Fig. 12. Table 2 shows the design parameter, value range, initial value, and optimized value of each parameter after the optimization of the flexibility calculation equation. The initial design value is optimized according to the flexibility closure equation. It can be seen from Table 1 that the changes of parameters before and after the parameter optimization are small, which also reflects the accuracy of the results of the flexibility calculation equation.

Table 3 lists the objective function values of gravity, assembly error, and temperature conditions before and after the parameter optimization. The optimal result obtained from the primary

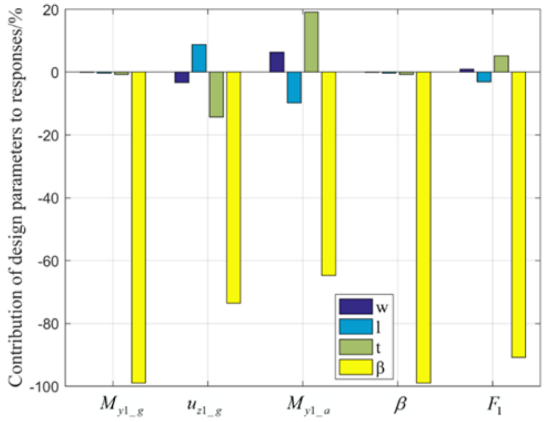

Fig. 12. Contributions of the design parameters to the target functions.

Table 2. Initial Values, Variation Range, and Optimal Values

Optimization Parameters	Initial Value/mm	Variation Range/mm	Optimal Value/mm
Thickness t	4.5	4–6	5
Width w	20	15–22	20
Length l	5	4–7	6
Included angle α	60°	50–65	60°

mirror assembly is shown in Fig. 13. As shown in Fig. 13, there is less astigmatism under the action of gravity. Astigmatism is dominant under 0.1 mm forced displacement, while the surface shape is dominated by trefoil astigmatism (similar to the form of Zernike's tenth term) under a temperature load. The design error budget is satisfied simultaneously. Considering that the different load cases are generally unrelated, the mirror surface accuracy under the combination of the transmitted loads can be calculated by the root sum square method. It can be seen from Table 3 that the first-order frequency of the mirror assembly reaches 129 Hz when the static design requirements are met. The first three modes of the assembly are shown in Fig. 14.

5. FLEXIBILITY VERIFICATION AND DYNAMIC PERFORMANCE ANALYSIS OF FLEXIBLE SUPPORT

A. Flexibility Verification of Flexible Support

As the processing cycles of the 2 m the SiC primary mirror is almost two years, the optical supporting performance of a flexure can hardly be verified in advance. However, with the presented method in this paper, the optical supporting performance can be estimated by testing the specific compliance of the flexure. Then the static and dynamic requirements of the flexure can be verified in advance.

In order to verify the accuracy of the flexible support design and simulation, the flexibility of the flexible support was measured experimentally. Figure 15 shows the translational flexibility C_{Z-F_z} test device of the flexible support. We place the dynamometer with force output accuracy of 0.5N on the three-dimensional adjustment frame to accurately control the

Table 3. Comparison of Responses before and after Parameter Optimization

Load Cases	Initial	Optimal
Gravity	$M_{y1} = 41482.1\ N \cdot \text{mm}$ RMS = 4.65 nm $u_{z1} = 12.4\ \mu\text{m}$	$M_{y1} = 41123.7\ N \cdot \text{mm}$ RMS = 4.65 nm $u_{z1} = 12.6\ \mu\text{m}$
0.1 mm assembly error	$M_{y1} = 1067.5\ N \cdot \text{mm}$ RMS = 3.56 nm $F_{z1} = 596.3\text{N}$	$M_{y1} = 1028.5\ N \cdot \text{mm}$ RMS = 3.43 nm $F_{z1} = 498.8\text{N}$
4°C temperature change	$M_{y1} = 26753.2\ N \cdot \text{mm}$ $\beta = \frac{M_{y1}}{F_{z1}} = 44.8$ RMS = 3.43 nm	$M_{y1} = 22185.4\ N \cdot \text{mm}$ $\beta = \frac{M_{y1}}{F_{z1}} = 44.5$ RMS = 3.4 nm
Frequency	130 Hz	129 Hz

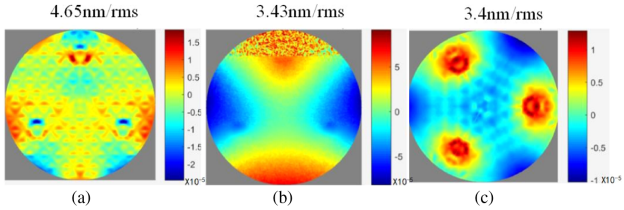

Fig. 13. Optimum result under three load cases. (a) 1 g gravity, (b) 0.1 mm assembly error, and (c) 4°C temperature change.

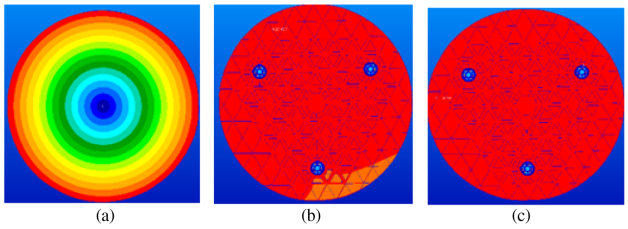

Fig. 14. Modal analysis result of the primary mirror assembly. (a) $f_1 = 129.3$, (b) $f_2 = 136.0$, and (c) $f_3 = 136.1$ Hz.

position of force application. First, we move the adjusting frame left and right to make the dynamometer output a force of 100N, and use the dial indicator to measure the translation of the flexible support end face many times. In order to verify the isotropy of the support, we remove the support from the tooling, rotate it 46 ° around the support axis (the rotation angle is related to the position of the screw hole at the constraint end of the flexible support), connect it with the tooling again, and measure the translation amount of the support under 100N force many times.

Figure 16 shows the rotating flexibility $C_{\theta_y - F_z}$ test device of the flexible support. We paste a small plane mirror on the end face of the flexible support, move the adjusting frame to make the dynamometer output a force of 100N, and measure the angle change of the plane mirror before and after the force was applied by Leica theodolite many times. Figure 17 shows the rotating flexibility $C_{\theta_y - M_y}$ test device of the flexible support. We apply 100N thrust and tension simultaneously through two identical dynamometers. Leica theodolite is used to measure the angle change of the plane mirror before and after the bending moment was applied many times. The flexibility measurement results are shown in Table 4. Comparing the simulation analysis

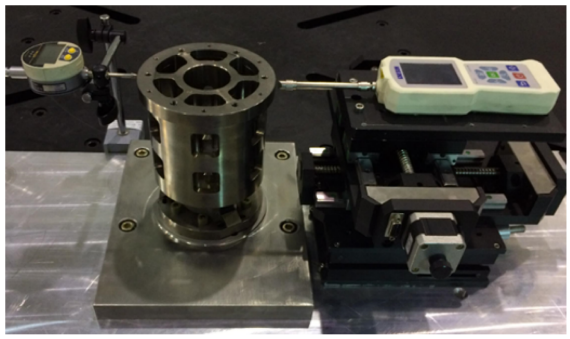

Fig. 15. Measuring device for translational compliance C_{Z-F_z}.

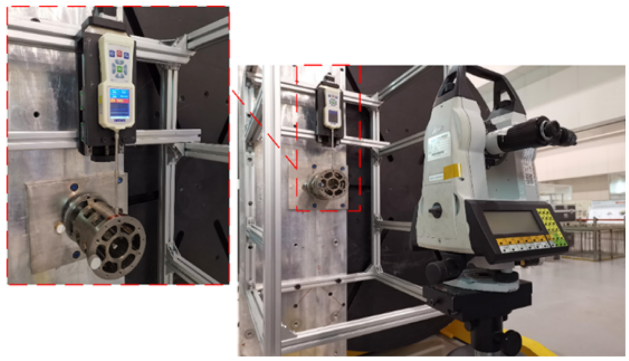

Fig. 16. Measuring device for rotational compliance $C_{\theta_y - F_z}$.

results with the experimental results, the measurement errors of C_{Z-F_z}, $C_{\theta_y - F_z}$, $C_{\theta_y - M_y}$ are all within 5%. The flexibility measurement results of the flexible support before and after the rotation angle are consistent, indicating that the flexible joint is isotropic. Table 5 shows the flexibility measurement results of the three flexible supports under the same state. The consistency of the three flexible supports is good.

B. Dynamic Performance Analysis of Flexible Support

When considering the dynamic performance of the flexible support, it is required that the dynamic stress must be less than the micro-yield strength of the material to ensure the structural stability of the mirror assembly. Otherwise, the flexible support may be permanently deformed, which will change the relative

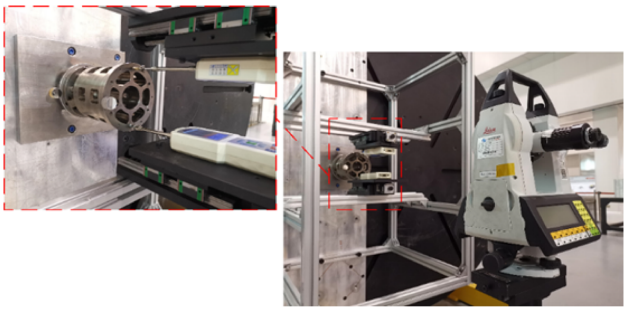

Fig. 17. Measuring device for rotational compliance $C_{\theta_y - M_y}$.

Table 4. Initial Values, Variation Range, and Optimum Values

Optimization	Test Location	Simulation Result	Experimental Result	Error
Flexibility	0°	0.165 mm	0.158 mm	4.43%
C_{Z-F_z}	46°	0.165 mm	0.157 mm	5.1%
Flexibility	0°	248.8″	244″	2%
$C_{\theta_y - F_z}$	46°	248.8″	241″	3.24%
Flexibility	0°	226.6″	221.5″	2.3%
$C_{\theta_y - M_y}$				

Table 5. Comparison of Compliance Measurement Results between Three Flexures

Material	Test Location	1#	2#	3#
Flexibility	0°	0.158 mm	0.158 mm	0.159 mm
C_{z-F_z}				
Flexibility	0°	244″	242″	241″
$C_{\theta_y - F_z}$				

position between the mirror components and affect the optical performance. We have verified the dynamic performance of the flexible support through a simulation analysis. Table 6 shows the excitation conditions of sinusoidal vibration, and the damping ratio is 0.03 based on engineering experience. The simulation analysis results of the primary mirror assembly in the X, Y, and Z directions are shown in Figs. 18(a)–18(c), respectively. The translational mode of the flexible support in the X direction is in the frequency band greater than 130 Hz, and the stress value in this frequency band increases exponentially. The upper boundary of the frequency of sine sweep is 100 Hz. At this time, the maximum stress of the flexible support in X, Y, and Z directions is 161.8, 240.2, and 242.3 Mpa respectively. The maximum stress points in three directions are located at the spring of the flexible support. The material of the flexible support is TC17, and the micro-yield stress is 672 Mpa (1120 Mpa × 60%).

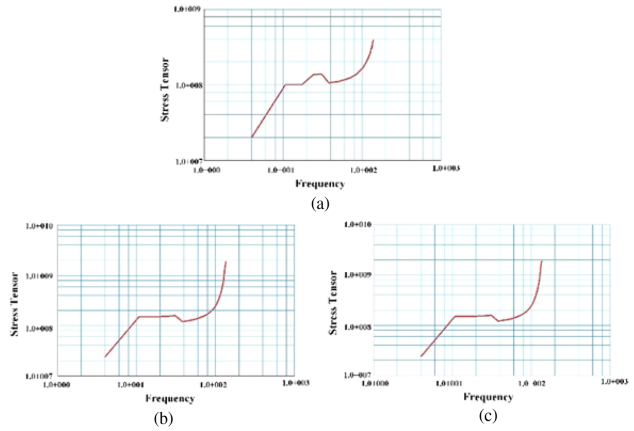

Fig. 18. Stress response of 2 m (PM) assembly under sinusoidal vibration in X/Y/Z directions.

Table 7. Summary of Measured Performance of Single Zernike Term

Loading Direction		X/Y/Z	
Frequency range (Hz)	10–50	50–800	50–800
Magnitude 0–p	3 dB/oct	0.032 g^2/Hz	0.032 g^2/Hz
RMS acceleration value		6.34 g	
Duration		2 min	

The results of the sinusoidal analysis show that the flexible supporting structure will not be deformed or destroyed. It meets engineering requirements.

Typically, the "3σ" criterion is used as the evaluation standard of random vibration response according to engineering experience. It assumes that the Gaussian distribution contains 99.7% of the response. The excitation conditions of random vibration are shown in Table 7. The random stress of the flexible support and the mirror surface node are shown in Figs. 19(a)–19(c). The maximum random stresses in X, Y, and Z directions are 455.7, 326.7, and 286.2 Mpa, respectively, and all the maximum stress points are located at the flexible support spring. The simulation results of random vibration show that the flexible support meets the engineering requirements.

6. CONCLUSION

Based on the back three-point support theory, an inverted tripod flexible support structure applied to a 2 m space primary mirror is proposed in this paper. First, according to the requirements of a 2 m primary mirror for flexible support flexibility, the 3PUU

Table 6. Summary of Measured Performance of Single Zernike Term

Loading Direction	X				Y/Z		
Frequency range	4–9	9–18	18–36	36–100	4–10	10–32	32–100
Amplitude 0–p	16.7 mm	5.4 g	7.2 g	5.4 g	18.0 mm	7.2 g	5.4 g
Load scan rate				2 oct/min			

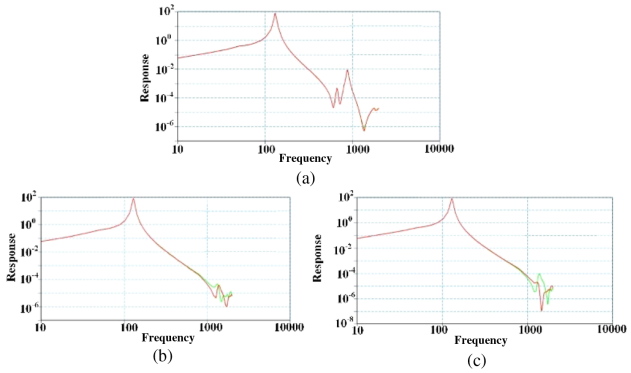

Fig. 19. Random vibration of PM assembly along X/Y/Z axes.

parallel flexible support topology was established. This structure can effectively release the rotational freedom, provide a certain translational flexibility, and yield high axial stiffness. According to the fast optimization model, the flexibility closed equation derivation and parameter optimization of 3PUU parallel flexible support were carried out. After the parameter optimization, the surface shape error and rigid body displacement under the horizontal gravity condition of the optical axis were 4.65 nm and 12.6 μm, respectively. The surface shape errors under a 0.1 mm assembly error condition and 4°C temperature condition were 3.43 and 3.4 nm, respectively. The first-order frequency of the mirror assembly reaches 129 Hz. The design results meet the design index requirements. The simulation results further verify the correctness of the flexibility equation. The flexibility characteristics of the flexible support were verified by the flexibility measurement test of the flexible support. With our method, the mirror design and flexure design were decoupled, and the independent evaluation of flexible support performance was realized.

Funding. National Natural Science Foundation of China (11703027).

Disclosures. The authors declare no conflicts of interest.

Data availability. Data underlying the results presented in this paper are not publicly available at this time but may be obtained from the authors upon reasonable request.

REFERENCES

1. P. Bely, *The Design and Construction of Large Optical Telescopes* (Springer-Verlag, 2003), pp. 1–28.
2. K. S. Park, J. H. Lee, and S. K. Youn, "Lightweight mirror design method using topology optimization," Opt. Eng. **44**, 053002 (2005).
3. R. Sahu, V. Patel, S. K. Singh, and B. S. Munjal, "Structural optimization of a space mirror to selectively constrain optical aberrations," Struct. Multidiscip. Optim. **55**, 2353–2363 (2017).
4. H. F. Hu, X. Luo, Z. Y. Liu, X. J. Zhang, D. Xue, and H. Zhao, "Designing a hydraulic support system for large monolithic mirror's precise in-situ testing-polishing iteration," Opt. Express **27**, 3746–3760 (2019).
5. X. Zhang, H. Hu, X. Wang, X. Luo, G. Zhang, W. Zhao, X. Wang, Z. Liu, L. Xiong, E. Qi, and C. Cui, "Challenges and strategies in high-accuracy manufacturing of the world's largest SiC aspheric mirror," Light Sci. Appl. **11**, 310 (2022).
6. N. Lobontiu, *Compliant Mechanisms: Design of Flexure Hinges* (CRC Press, 2002).
7. S. T. Smith, V. G. Badami, J. S. Dale, and Y. Xu, "Elliptical flexure hinges," Rev. Sci. Instrum. **68**, 1474–1483 (1997).
8. N. Lobontiu, E. Garcia, M. Hardau, and N. Bal, "Stiffness characterization of corner-filleted flexure hinges," Rev. Sci. Instrum. **75**, 4896–4905 (2004).
9. N. Lobontiu, J. S. Paine, E. Garcia, and M. Goldfarb, "Corner-filleted flexure hinges," J. Mech. Des. **123**, 346–352 (2001).
10. N. Lobontiu, J. S. N. Paine, E. Garcia, and M. Goldfarb, "Design of symmetric conic-section flexure hinges based on closed-form compliance equations," Mech. Mach. Theory **37**, 477–498 (2002).
11. N. Lobontiu and E. Garcia, "Analytical model of displacement amplification and stiffness optimization for a class of flexure-based compliant mechanisms," Comput. Struct. **81**, 2797–2810 (2003).
12. B. Shusheng, Z. Hongzhe, and Y. Jingjun, "Modeling of a cartwheel flexural pivot," J. Mech. Des. NY **131**, 061010 (2009).
13. B. Inlan, "Influence of axial-force errors on the deformation of the 4 m lightweight mirror and its correction," Appl. Opt. **56**, 611–619 (2017).
14. H. Kihm, H. S. Yang, I. K. Moon, J. H. Yeon, S. H. Lee, and Y. W. Lee, "Adjustable bipod flexures for mounting mirrors in a space telescope," Appl. Opt. **51**, 7776–7783 (2012).
15. B. Eiliu, "Design of an adjustable bipod flexure for a large-aperture mirror of a space camera," Appl. Opt. **57**, 4048–4055 (2018).
16. M. Kotani, T. Imai, H. Katayama, Y. Yui, Y. Tange, H. Kaneda, T. Nakagawa, and K. Enya, "Quality evaluation of space-borne SiC mirrors (I): analytical examination of the effects on mirror accuracy by variation in the thermal expansion property of the mirror surface," Appl. Opt. **52**, 4797–4805 (2013).
17. P. W. Zhou, S. Y. Xu, C. X. Yan, and X. H. Zhang, "Research on neutral surface of lightweight, horizontally supported mirror," Opt. Eng. **57**, 025107 (2018).
18. R. W. Besuner, K. P. Chow, S. E. Kendrick, and S. Streetman, "Selective reinforcement of a 2m-class lightweight mirror for horizontal beam optical testing," Proc. SPIE **7018**, 701816 (2008).
19. Y. Y. Yui, K. Goto, H. Kaneda, H. Katayama, M. Kotani, M. Miyamoto, M. Naitoh, T. Nakagawa, H. Saruwatari, M. Suganuma, and H. Sugita, "Performance of lightweight large C/SiC mirror," Proc. SPIE **10566**, 105660M (2017).
20. X. Liu, X. Tian, W. Zhang, B. Zhang, Z. Cheng, L. Fu, and Z. Wang, "Lightweight design of high volume SiC/Al compo-site mirror for remote camera," Optik **188**, 64–70 (2019).
21. R. Hu, S. T. Liu, and Q. H. Li, "Topology-optimization-based design method of flexures for mounting the primary mirror of a large-aperture space telescope," Appl. Opt. **56**, 4551–4560 (2017).
22. P. W. Zhou and S. Xu, "Fast optimal design of a flexure for lightweight, horizontally supported mirror," J. Astron. Telesc. Instrum. Syst. **5**, 024001 (2019).
23. P. Jiang and P. W. Zhou, "Optimization of a lightweight mirror with reduced sensitivity to the mount location," Appl. Opt. **59**, 3799–3805 (2020).
24. L. Howell, *Compliant Mechanisms* (Wiley, 2001).
25. S. Xiao, Y. Li, and X. Zhao, "Optimal design of a novel micro-gripper with completely parallel movement of gripping arms," in *IEEE Conference on Robotics, Automation and Mechatronics (RAM)* (IEEE, 2011).
26. S. Xiao, Y. Li, and Q. Yang, "A novel flexure-based 3-DOF micro-parallel manipulator with gripper for micro/nano manipulation," in *6th IFAC Symposium on Mechatronic Systems (Mechatronics)*, Hangzhou, China, IFAC, 2013, Vol. **46**, pp. 606–611.
27. H. Kihm, H. S. Yang, and Y. W. Lee, "Bipod flexure for 1-m primary mirror system," Rev. Sci. Instrum. **85**, 125101 (2014).
28. L. C. Hale, "Principles and techniques for designing precision machines," Ph. D. thesis (Lawrence Livermore National Laboratory, 1999), pp. 304–305.
29. P. Zhou, K. Wang, C. Yan, and X. Zhang, "Research on the degradation of lightweight mirror surface accuracy," Appl. Opt. **57**, 7758–7763 (2018).